# Ion Specificity in α-Helical Folding Kinetics

**Yann von Hansen, Immanuel Kalcher, and Joachim Dzubiella***

*Physics Department T37, Technical University Munich, 85748 Garching, Germany*

*Received: August 9, 2010; Revised Manuscript Received: September 16, 2010*

The influence of the salts KCl, NaCl, and NaI at molar concentrations on the α-helical folding kinetics of the alanine-based oligopeptide Ace-AEAAAKEAAAKA-Nme is investigated by means of (explicit-water) molecular dynamics simulations and a diffusional analysis. The mean first passage times for folding and unfolding are found to be highly salt-specific. In particular, the folding times increase about 1 order of magnitude for the sodium salts. The drastic slowing can be traced to long-lived, compact configurations of the partially folded peptide, in which sodium ions are tightly bound by several carbonyl and carboxylate groups. This multiple trapping leads to a nonexponential residence time distribution of the cations in the first solvation shell of the peptide. The analysis of α-helical folding in the framework of diffusion in a reduced (one-dimensional) free energy landscape further shows that the salt not only specifically modifies equilibrium properties but also induces kinetic barriers due to individual ion binding. In the sodium salts, for instance, the peptide's configurational mobility (or "diffusivity") can decrease about 1 order of magnitude. This study demonstrates the highly specific action of ions and highlights the intimate coupling of intramolecular friction and solvent effects in protein folding.

## 1. Introduction

The complex problem of protein folding is typically interpreted in terms of a diffusive search through an effective, low-dimensional free energy landscape, where most of the countless degrees of freedom of the system have been integrated out.[1−6] In this scenario the effective diffusivity (or friction) arising from intrapeptide and peptide−solvent interactions as well as from orthogonal degrees of freedom varies considerably along the reaction coordinate (RC).[7,8] In general, the internal friction constitutes a major contribution to the friction, such that solvent viscous drag and solvent−peptide interactions are not the only mechanisms that govern protein kinetics.[9,10] Internal and solvent-induced friction processes may even be intimately connected as was demonstrated for the loop formation rate of unfolded peptides, where the strongly denaturing salt guanidine hydrochloride modifies internal friction by specific binding mechanisms.[11,12]

The investigation of the salt-specific action on proteins in general ('Hofmeister effects') has a long history,[13] but the underlying mechanisms are still under exploration. In a recent series of experiments, for example, it has been shown that even the simple cations sodium ($Na^+$) and potassium ($K^+$) exhibit considerably different behavior in the interaction with protein surfaces, where $Na^+$ is favored over $K^+$.[14−16] One apparent reason is the stronger attraction of sodium to acidic (anionic) surface groups, in particular to carbonyl and side chain carboxylate groups. While these static properties have received much attention lately,[17] not much is known about their consequences to biomolecular kinetics. Experimental hints have been given in studies of $Na^+$- and $K^+$-specific polyglutamic acid aggregation kinetics,[18] folding kinetics of halophilic ('salt-loving' and very acidic) proteins,[19,20] or DNA.[21] However, a detailed molecular understanding of the ion-specific action on biomolecular folding and assembly kinetics is still lacking.

In particular for large concentrations ($c \gtrsim 1$ M), salt effects are pronounced, highly sequence and salt-type specific; they typically lead to changes in protein solubility, stability, and/or denaturation that result in the so-called Hofmeister series for the precipitation of proteins.[13] Although 1 order of magnitude higher than at typical physiological conditions ($c \sim 0.2$ M), large salt concentrations play a central biochemical role in the broad field of protein crystallization,[22] in food industry as fermentation additives,[23] and for the function and stability of biotechnologically interesting halophilic (salt-loving) enzymes.[24] Additionally, the study of protein structures in solvents with high salinity is instructive, as salt-specific effects are amplified and, important from a computational perspective, can be sampled more efficiently in molecular dynamics (MD) simulations, a popular tool nowadays for the theoretical study of protein folding, function, and stability.[25]

A ubiquitous and fundamental secondary structure element of proteins is the α-helix, which is stabilized by $(i, i + 4)$ backbone hydrogen bonds involving four amino acids (aa) per turn. The majority of short ($\lesssim$20 aa) isolated helices derived from proteins are unstable in solution, unless specific side-chain interactions stabilize them. Among those it has been demonstrated that alanine-based peptides have the strongest intrinsic helix propensity.[26−30] A very instructive model peptide experimentally introduced by Marqusee and Baldwin[26] showed that alanine-based oligopeptides with an $A(EAAAK)_nA$ pattern display a high α-helix propensity, which is probably stabilized by $Glu^-$ (E) and $Lys^+$ (K) salt bridges along the folded peptide. Marqusee and Baldwin also found that the simple salt NaCl has a destabilizing effect on the α-helical configurations of these peptides.

Indeed, in a recent explicit-water molecular dynamics (MD) computer simulation[31] the structural behavior of the oligopeptide Ace-AEAAAKEAAAKA-Nme, in the following named the 'EK' peptide, has been explored in detail, and the stabilizing and destabilizing mechanisms in various highly concentrated aqueous electrolyte solutions have been identified. Among those

* To whom correspondence should be addressed. E-mail: jdzubiel@ph.tum.de.

10.1021/jp107495f 
Published on Web 10/13/2010

it has been found that sodium ($Na^+$) destabilizes the helical structure more strongly than potassium ($K^+$); it was also previously recognized that the reason for the destabilization of the salt bridges and the hydrogen bonds of the secondary structure lies in the higher affinity of $Na^+$ to carboxylate and carbonyl groups. In a recent follow-up paper the folding kinetics of the EK-peptide in pure aqueous solution was investigated and interpreted in terms of diffusion in a reduced (one-dimensional) free energy landscape involving a local coordinate-dependent diffusivity.[8]

The aim of this work is to extend these previous studies on the 'EK'-peptide to the investigation of the specific effects of the salts KCl, NaCl, and NaI on peptide α-helical *folding and unfolding kinetics*. In particular, we explore how salts alter the mean folding and unfolding times and look for possible molecular reasons. Strong salt-specific effects are found in the mean folding times, which can be attributed to the binding of individual ions to multiple, anionic peptide groups inducing transient cross-links between peptide fragments. In consequence, not only equilibrium distributions of configurations are modified but also new, slow time scales in the peptide's configurational mobility arise due to enhanced internal friction. Salt effects are thus reflected in both modified free energy landscape and local changes of the effective diffusivity. Our study demonstrates the highly specific action on protein folding kinetics by the individual binding of ions and, more generally, exemplifies the intimate coupling between solvent and intrapeptide friction effects in protein folding. We believe that these mechanisms could be of general importance and transferable to a variety of biomolecular and polyelectrolyte systems.

## 2. Methods

**A. MD Simulations.** Our MD simulations are performed using the parallel module *sander.MPI* in the simulation package Amber9.0 with the ff03 force field for the peptides and the rigid and nonpolarizable TIP3P water for the solvent.[32] All simulated systems are maintained at a fixed pressure of $P = 1$ bar and a temperature $T = 300$ K by coupling to a Berendsen barostat and Langevin thermostat,[32] respectively. The cubic and periodically repeated simulation box of edge length $L \simeq 36$ Å includes approximately 1500 water molecules. Electrostatic interactions are calculated by particle mesh Ewald summation, and all real-space interactions (electrostatic and van der Waals) have a cutoff of 9 Å. The peptide is generated using the *tleap* tool in the Amber package.[32]

We investigate the helical folding and unfolding behavior of a 12 amino acid long peptide with the acetyl (Ace) and amine (Nme) capped sequence Ace-AEAAAKEAAAKA-Nme. This peptide can form three α-helical turns in the fully folded state, where Glu2 and Lys6, and Glu7 and Lys11, are potentially able to form a salt bridge, respectively.[31] The influence on α-helix folding kinetics of a large concentration of $\simeq 3.6 \pm 0.1$ M of the simple monovalent salts NaCl, KCl, and NaI is investigated. We have simulated the system without salt for $\simeq 1.35$ $\mu$s and including salt for $\simeq 2$ $\mu$s for each salt type. We note here that the free energy along the RC $q$ (see below) derived from replica-exchange MD trajectories at $T = 300$ K for the salt-free system gives very good agreement to the brute force approach,[8] indicating a decent statistical sampling by our trajectories.

The considered salt concentrations result from 90 ion pairs in the simulation box. Cations and anions are modeled as nonpolarizable Lennard−Jones spheres with charge and interaction parameters as supplied by Dang,[33] as the default Amber parameters are known to be faulty.[34] The Dang parameters show reasonable bulk thermodynamic properties in SPC/E water even for high concentrations.[35] Comparative calculations (unpublished) in TIP3P water show only small differences in hydration structure, and no qualitative difference in the binding to peptide groups.[36] The parameters used are summarized in previous work on the equilibrium structure of the EK peptide in salt at a different temperature.[31] We are aware of the weaknesses of ionic MD force fields for quantitative predictions in biomolecular simulations; this issue has already been discussed in our previous study, where however a reasonable description of helicity and destabilization with NaCl was observed when compared to experiments. Since the destabilization seems to be overemphasized for NaCl, we do not claim to be quantitative in our work but focus rather on the discussion of the main effects and qualitative trends with the addition of salt; we believe these to be insensitive to the particular force field and relevant for a variety of experimental observations.

**B. Helicity and Reaction Coordinate.** Trajectory analysis is performed using the *ptraj* tool in the Amber9.0 package.[32] The helicity, i.e., the α-helical fraction, is identified using the DSSP method by Kabsch and Sander.[37] We focus on one RC $Q$, which is defined as the root-mean-square distance from a fully helical reference structure (i.e., with helicity equal to one), averaged over all atoms of the peptide and which thus measures the deviation from the 'native' state; this quantity was previously found to act as an adequate dynamic RC in the salt-free case.[8] We note that different choices of the reference structure were tested and resulted only in small differences in the energy landscapes, i.e., local variations on the order of fractions of the thermal energy $k_BT$; see Supporting Information for additional details. Similarly, the RC-trajectories only marginally change when varying the reference structure and therefore yield the same kinetic behavior; examples of such trajectories are also found in the Supporting Information. Trajectories are recorded with a resolution of 20 ps, giving a total of ∼67 500 data points for the simulations without salt and roughly 100 000 data points for the runs including salt. For convenience, we define a rescaled RC by $q = (Q - Q^{min})/(Q^{max} - Q^{min})$ such that the minimal and maximal values of the data points, denoted as $Q^{min}$ and $Q^{max}$, are projected on the RC values $q = 0$ and $q = 1$, respectively. The absolute minimum and maximum RC values are similar for all systems and are $Q^{min} \simeq 1.0$ Å and $Q^{max} \simeq 8.0$ Å.

**C. Bulk Shear Viscosities.** In order to get a more complete picture of the solvent properties, we calculate bulk shear viscosities for NaCl, KCl, and NaI at the relevant concentrations in TIP3P water. We employ the same ionic force fields as above but perform the simulations with the GROMACS 4.0[38,39] package due to the implemented viscosity calculation methods. In these simulations, the periodically repeated box has an edge length of $L \simeq 4$ nm, with a total number of $N_w = 1910$ water molecules and $N_i = 135$ ion pairs. For the pure water simulation we use $N_w = 2180$ water molecules. After *NPT*-equilibration we proceed with an *NVT*-production run of 50 ns. We compare two approaches to calculate the viscosity: first, we employ the Green−Kubo (GK) formula[40,41]

$$\eta = \frac{V}{k_BT}\int_0^\infty \langle P_{xz}(t_0)P_{xz}(t_0 + t)\rangle_{t_0} \mathrm{d}t \qquad (1)$$

involving the off-diagonal components of the pressure tensor only. We obtained averaged viscosities over a correlation time of 5 to 20 ps. The latter choice reflects the fact that the viscosity converges rapidly but exhibits large statistical errors for long correlation times.[42]

Second, we perform a nonequilibrium perturbation method.[40] In this scheme, an external force is applied in the *NVT*-simulation with the periodic acceleration profile

$$a_x(z) = A\cos(kz) \tag{2}$$

with $k = 2\pi/L$, $L$ being the edge length of the box. The amplitude $A$ should be chosen small enough in order not to drive the system out of the linear response regime and at the same time large enough to get good statistics. For a more detailed discussion we refer to previous work[40] and set the amplitude to $A = 0.02$ nm ps$^{-2}$. We then obtain the viscosity by calculating the average velocity profile of all particles.[40]

With the GK formula we find values of $\eta_0 = 0.31 \pm 0.01 \times 10^{-3}$ kg/(m·s) for pure TIP3P water, corroborating with previous studies,[43] and $\eta = 0.58$, 0.74, and $0.6 \pm 0.01 \times 10^{-3}$ kg/(m·s) for the KCl, NaCl, and NaI solutions at a concentration of 3.6 mol/l, respectively. The periodic perturbation method yields the same results within a 5% error range. Compared to experimental values[44] the MD simulation considerably overemphasizes the increase of the viscosity at this elevated salt concentration; indeed, the viscosity was experimentally found to increase by only roughly 5% for KCl and 30−40% for NaCl and NaI compared to pure water. This failure in describing the correct bulk viscosities of the electrolyte solutions must be attributed to inaccuracies in the force field. Note that the value for pure TIP3P water already considerably deviates from the experimental value ($0.893 \times 10^{-3}$ kg/(m·s) at 298.15 K)[45] by more than a factor of 2.

**D. Free Energy and Diffusivity Profiles.** We assume that the stochastic time evolution of the probability $\Psi(q, t)$ of finding a configuration with RC value $q$ at time $t$ is described by the one-dimensional Fokker−Planck (FP) equation[46]

$$\frac{\partial}{\partial t}\Psi(q,t) = \frac{\partial}{\partial q}D(q)\mathrm{e}^{-\beta F(q)}\frac{\partial}{\partial q}\Psi(q,t)\mathrm{e}^{\beta F(q)} \tag{3}$$

where $D(q)$ is the (in general $q$-dependent) diffusivity, $\beta \equiv 1/(k_\mathrm{B}T)$, and $F(q) = -k_\mathrm{B}T\ln\langle\Psi(q)\rangle$ is the free energy obtained by Boltzmann-inversion of the time-averaged probability distribution $\langle\Psi(q)\rangle$. We employ a recently introduced method to estimate the diffusivity profile that takes advantage of the relation between average transition times between different points along the RC, the free energy landscape $F(q)$, and the diffusivity profile $D(q)$.[8] The round-trip time defined as

$$\tau_\mathrm{RT}(q, q_\mathrm{t}) \equiv \mathrm{sign}(q - q_\mathrm{t})[\tau_\mathrm{fp}(q, q_\mathrm{t}) + \tau_\mathrm{fp}(q_\mathrm{t}, q)] \tag{4}$$

specifies the average time needed for an excursion starting at $q$, reaching $q_\mathrm{t}$ at least once, and returning to $q$ for the first time; mean first passage times for transitions starting at $q$ and reaching $q_\mathrm{t}$ are denoted by $\tau_\mathrm{fp}(q, q_\mathrm{t})$. For a diffusive process described by the FP eq 3, the round-trip time is given by the integral

$$\tau_\mathrm{RT}(q, q_\mathrm{t}) = \int_{q_\mathrm{t}}^{q} \mathrm{d}q' \frac{1}{D(q')\langle\Psi(q')\rangle} \tag{5}$$

which can be derived from the expressions for the mean first passage time given previously.[8] Though eq 5 can in principle be inverted to obtain the diffusivity profile $D(q)$ from the slope of the round-trip time curves, we choose a complementary analysis method within the present work to avoid artifacts due to insufficient statistical sampling. The FP approach assumes an underlying Markovian process and, as is easily seen from eq 5, round-trip time curves (as a function of $q$) for different target points $q_\mathrm{t}$ therefore only differ by a constant

$$\tau_\mathrm{RT}(q, q_\mathrm{t}) = \tau_\mathrm{RT}(q, q_\mathrm{t}') + \tau_\mathrm{RT}(q_\mathrm{t}', q_\mathrm{t}) \tag{6}$$

The assumption of Markovian behavior however generally breaks down at short times and for unsuitable RCs, i.e., RCs that do not single out the transition state; see also previous literature on that topic.[8]

In our analysis of the simulation time series $q(t)$ we discretize the RC in $N = 50$ intervals centered around $q^{(i)} = (2i - 1)/100$, $i \in \{1, 2, ..., 50\}$; mean first passage times between all possible pairs of bins are extracted from simulation data and converted into round-trip times using eq 4. To simplify the analysis, we assume a flat diffusivity within each of the following regions: (i) values of the RC $q < q_{2/3}$ corresponding to an almost perfectly folded helix, (ii) one or two unfolded helical turns equivalent to $q_{2/3} \le q < q_{1/3}$, and (iii) mostly unfolded states characterized by RC values $q \ge q_{1/3}$, where the indices 1/3 and 2/3 denote the average helicity at these $q$ values. The values of the diffusivity in those three regions are used as fit parameters in eq 5 to best reproduce the round-trip time curves obtained from simulation data; the integral in eq 5 is computed numerically by linear interpolation of $\{\langle\Psi(q^{(i)})\rangle\}_{i=1}^{50}$. Best fits to the round-trip data for different target points $q_\mathrm{t}$ allow the determination of the diffusivity (including an error estimate) in each of the three regions. Alternatively, the diffusivity profile can also be obtained by fitting to the average round-trip time

$$\bar{\tau}_\mathrm{RT}(q^{(j)}) \equiv \frac{1}{N}\sum_{i=1}^{N}\tau_\mathrm{RT}(q^{(j)}, q^{(i)}) \tag{7}$$

which is less affected by statistical noise and which according to eq 6 is just shifted vertically with respect to the round-trip curve $\tau_\mathrm{RT}(q, q_\mathrm{t})$ for a specific target position $q_\mathrm{t}$. The results of both fitting procedures are shown and discussed in section 3C, and additional information concerning the fitting is provided in the Supporting Information.

## 3. Results and Discussion

**A. Equilibrium Free Energy Landscapes.** The RC time series $q(t)$ of all investigated systems is shown in Figure 1: numerous folding and unfolding transitions on different time scales are discernible. Already at a first glance longer time scales (and fewer folding and unfolding transitions) seem to be involved in the systems with the sodium salts, which will be quantified and discussed in more detail later. Free energy profiles $F(q)$ of all investigated systems are extracted from the trajectories $q(t)$ and plotted in Figure 2 together with the (time-averaged) helicity resolved along the RC $q$. In the salt-free case (black curve) in Figure 2a, three minima are clearly visible: one at $q_1 \simeq 0.1$, a second at $q_2 \simeq 0.32$, and a third, shallow one at $q_3 = 0.58$. Judging from the helicity vs $q$, plotted in Figure 2b, these minima seem to correspond mainly to (1) a full helix with three turns, (2) a partially unfolded helix with two neighboring turns, and (3) one helical turn as well as fully unfolded states. Representative simulation snapshots taken at corresponding $q_i$ values ($i = 1, 2, 3$) confirm this view and are also shown in Figure 2b. We note that the value of $q_1$, which in

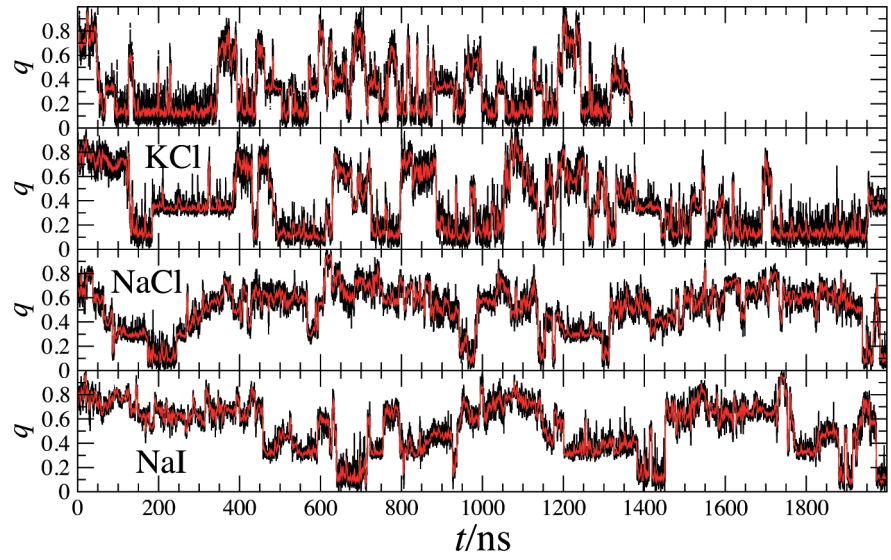


**Figure 1.** Time series data for reaction coordinate $q$ from the MD simulations in explicit salt water with varying salt type. Data in black shows the full 20 ps resolution, while data in red is smoothed over time windows of 2 ns.

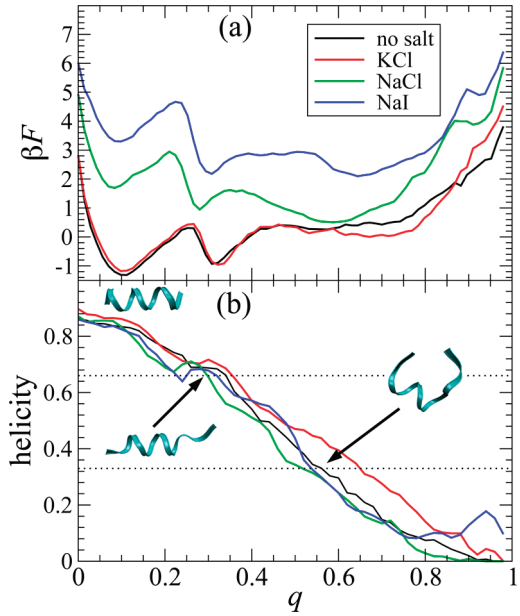


**Figure 2.** (a) Free energies $F(q)$ for the EK peptide in different salt solutions; the profiles are shifted vertically for better comparison. (b) Average α-helicity of the peptide resolved by $q$. The snapshots illustrate the backbone structure of partially folded−unfolded states corresponding to values of the helicity indicated by arrows. Simulation snapshots are visualized using VMD.[55]

absolute units corresponds to $Q_1 \simeq 1.6$ Å, deviates from 0 (the reference state) due to thermal fluctuations.

For KCl, the free energy $F(q)$ is slightly shifted to favor unfolded states at larger $q$ values ($q_3 \simeq 0.67$), while the main features remain the same as without salt. The total helicity decreases slightly from 62% to 55%. For the sodium salts, NaCl and NaI, the fully folded state at $q_1$ becomes metastable, and the distribution is strongly shifted to the partially and fully unfolded states. In particular, the third minimum at $q_3$ deepens and broadens. Also in the systems with salt the minima mostly match with partially folded α-helical states as can be judged from the helicity vs $q$ curve. All total helicities and positions of the minima in $F(q)$ are summarized in Table 1.

For the NaCl and NaI salts the total helicity significantly decreases to about 39% and 34%, respectively. The main causes

**TABLE 1: Total Helicity of the Investigated Systems and Distinct Positions in the Free Energy Landscape Shown in Figure 2**[a]

| system | helicity | $q_1$ | $q_2$ | $q_3$ | $q_{2/3}$ | $q_{1/3}$ |
|---|---|---|---|---|---|---|
| no salt | 0.62 | 0.11 | 0.31 | 0.57 | 0.34 | 0.56 |
| KCl | 0.55 | 0.10 | 0.32 | 0.67 | 0.35 | 0.65 |
| NaCl | 0.39 | 0.08 | 0.28 | 0.59 | 0.30 | 0.52 |
| NaI | 0.34 | 0.09 | 0.31 | 0.65 | 0.32 | 0.53 |

[a] Locations of local minima are denoted by $q_i, i = 1, 2, 3$, and values of the RC, where the average helicity is 2/3 or 1/3, by $q_{2/3}$ and $q_{1/3}$, respectively.

have been discovered previously[31] and are 2-fold: first, specific $Na^+$-binding to the glutamic acid side chain carboxylates interferes with EK salt bridging, and second, the binding of cations to backbone carbonyls perturbs the hydrogen bonds of the secondary structure.[31] In comparison to $Na^+$, the specific binding of $K^+$ is weak, and thus KCl is less destabilizing. We note that quantitatively these effects are force field dependent while the binding trends have been corroborated in many experiments and various simulation studies.[14−16] For completeness, we plot radial distribution functions (rdfs) between the cations and the oxygen atoms from the backbone carbonyls and side chain carboxylates in Figure 3: the dominance of sodium over potassium binding to the anionic peptide groups is obvious.

**B. Long-Lived Structures and Specific Ion Binding.** Previous work on the EK−peptide stability in salt solution[31] revealed that due to $Na^+$-binding *long-lived* loop-forming configurations occupy the region of intermediate to large $q$ values, in addition to one-turn and random coil states also present without salt. In these looped configurations a single $Na^+$ ion is collectively trapped by a few peptide backbone carbonyls and side chain carboxylates. This leads to a partial wrapping of the oligomeric backbone around the ion. From a superficial inspection of our trajectories we find that these long-lived configurations involving tightly bound $Na^+$ ions can be stable on a ≃1−10 ns time scale. Representative simulation snapshots which are dynamically selected such that they exist for more than 2 ns are shown in Figure 4: in panel a the sodium ion is bound and wrapped by the central part of the peptide, while the terminal parts exhibit partial helical turns. The bound sodium 'locks' this structure on times up to several nanoseconds. Similar long-lived situations are found, where two neighboring turns are correctly folded,

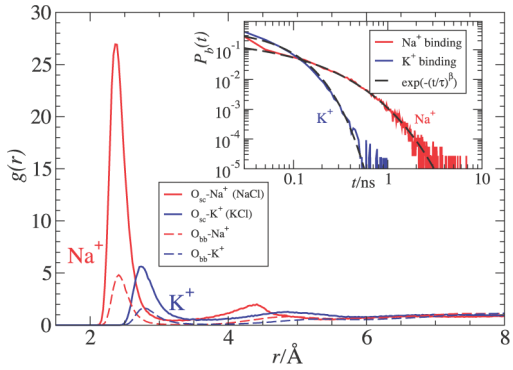


**Figure 3.** Radial distribution function of cations around peptide oxygen atoms from the side chain (sc) carboxylates or backbone (bb) carbonyls. Inset: residence time distribution for the cations in the first solvation shell of the peptide oxygen atoms. The distribution for $K^+$ can be fitted by a single exponential with a time constant of $\tau = 50$ ps, while the distribution for $Na^+$ obeys a stretched exponential with $\tau = 50$ ps and stretching exponent $\beta = 0.55$.

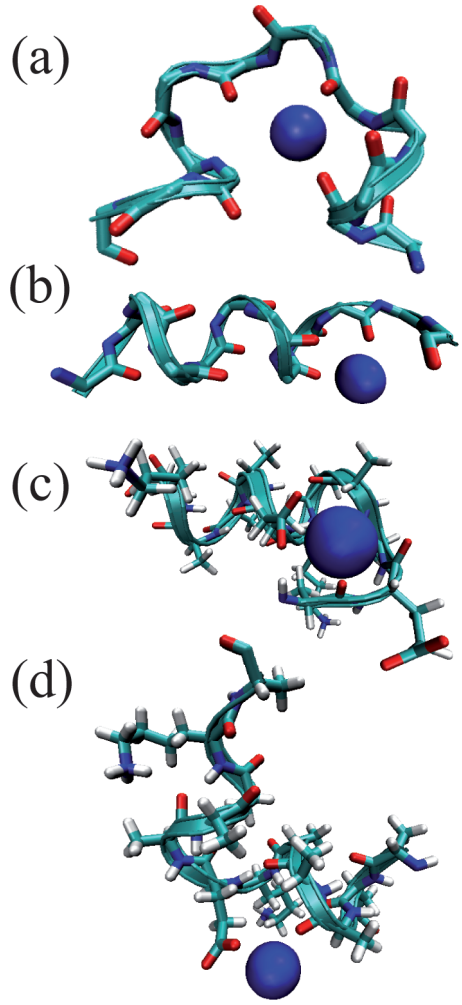


**Figure 4.** Simulation snapshots of backbone configurations, in which a single $Na^+$ ion (blue sphere) is trapped by multiple oxygen binding sites (red). These snapshots are dynamically selected such that the shown configurations existed for longer than 2 ns. In a and b no side chains are shown, to better illustrate the binding to the backbone. In c and d all side chains are shown. Here, also glutamic acid side chains are involved in binding the cation.

while the rest of the peptide forms a loop around the cation (see Figure 4b). Often also the glutamic acid side chain is involved as displayed in Figure 4c and 4d where the cation not only binds to a backbone carbonyl but also to the headgroup of the $E^-$ side chain. In all these situations the peptide is relatively compact with one or two turns correctly folded such that the relevant $q$ region of these states is between $0.25 \lesssim q \lesssim 0.65$, where the helicity is mostly between 2/3 and 1/3 (cf. Figure 2b). Configurations of this type have not or only rarely been found involving anions or a $K^+$ ion, so that their existence must be attributed to the relatively strong binding of the $Na^+$ ion.

The rigorous lifetime analysis of the occurring configurations involving trapped ions is difficult to perform because of the variety and complexity of the somewhat amorphous structures. We therefore resort to the analysis of cation binding times. In the inset to Figure 3, we plot the binding time distribution $P_b(t)$ of the cations $K^+$ and $Na^+$ in the first solvation shell of carboxylates and carbonyls (defined by the location of the first minimum in the cation rdfs in Figure 3). While the distribution decays exponentially for $K^+$ with a time constant of about 50 ps, we find a much slower, nonexponential behavior for $Na^+$ which can be best fitted by a stretched exponential of the form $\propto \exp(-t/\tau)^\beta$ with $\tau \simeq 50$ ps and $\beta = 0.55$. This indicates that long binding times on the order of nanoseconds are indeed possible and corroborate the existence of 'trapped' unfolded configurations in which peptide parts tightly wrap around the cation.

We note that it is indeed well established that systems with multiple trapping or other manifestations of disorder can lead to anomalous kinetics.[47] In our investigated systems, the appearance and magnitude of trapping is controlled by the nature of the ions. The observed 'stretched' exponentials resemble the slow relaxation in glass-forming liquids.[48] Anomalous kinetics in peptide and protein dynamics have been indeed observed in simulations and experiments for certain dynamic variables or RCs[49−51] and obviously question the general validity of diffusive approaches to predict long time dynamics in protein folding. While this complex issue is still awaiting resolution we proceed in this work with the interpretation of helix folding in the framework of simple diffusion; since the average folding/unfolding times ($\gtrsim$10 ns) are typically much larger than the ion binding times ($\sim$50 ps), we expect the long-term dynamics to be adequately described in terms of memoryless diffusion in a free energy landscape.

**C. Folding Kinetics and Diffusional Analysis.** Let us first analyze mean folding and unfolding times. In Figure 5a we plot the mean first passage time for folding from $q > q_1$ to $q_1$ given by $\tau_f(q, q_1) \equiv \tau_{fp}(q, q_1)$; the salt-specific values of $q_1$ are found in Table 1. Without salt the typical folding time is about $\tau_f \simeq 20-30$ ns in the region $q \gtrsim 0.3$ before it quickly drops down to 0 for $q$ values closely approaching $q_1$. In KCl $\tau_f(q, q_1)$ increases by a factor of about 2 while the sodium salts lead to a considerable slowing of folding by 1 order of magnitude. The unfolding times $\tau_{uf}(q, q_3)$ $(q < q_3)$, cf. Figure 5b, show less variations between the salts. Without salt the typical unfolding time is about 30−40 ns while it may rise by a factor of 2−3 in NaCl or KCl. Note that for KCl the unfolding is considerably slower than in the salt-free case although the free energy landscape is very similar.

To get a grasp on the folding kinetics involving fewer helical turns we have also analyzed $\tau_f(q, q_2)$ for $q > q_2$ (folding by one or two turns to the two-turn state) and $\tau_{uf}(q, q_2)$ for $q < q_2$ (unfolding by one turn to the two-turn state), which are shown in Figure 6a and 6b, respectively. The folding times decrease by a factor of about 2 when compared to the $q \rightarrow q_1$ folding, while the trends with salt remain the same, in particular a 1 order of magnitude slower folding in the sodium salts. Unfolding

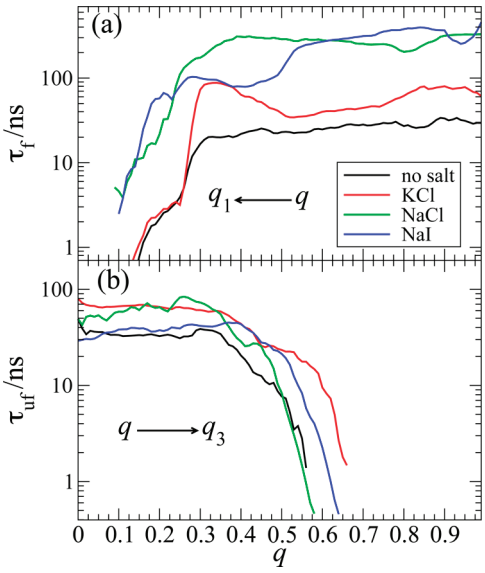


**Figure 5.** (a) Mean first passage times $\tau_f$ for folding from state $q$ to $q_1$. (b) Mean first passage times $\tau_{uf}$ for unfolding from state $q$ to $q_3$.

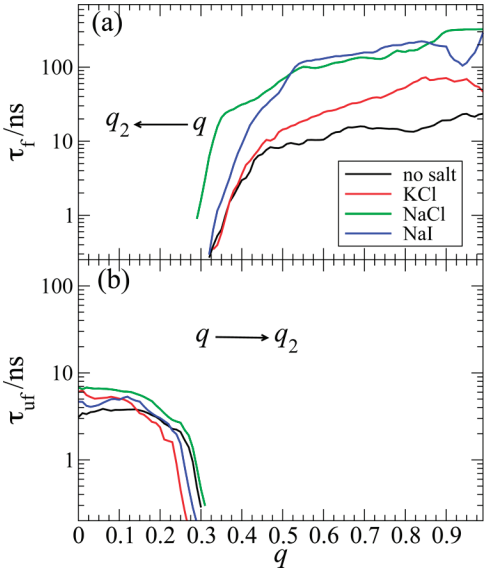


**Figure 6.** (a) Mean first passage times $\tau_f$ for folding to state $q$ to $q_2$. (b) Mean first passage times $\tau_{uf}$ for unfolding to state $q$ to $q_2$.

times $\tau_{uf}(q, q_2)$ are relatively small and found between 3−7 ns. The variation between the salts is again less pronounced for unfolding when compared to the folding times and show a different ordering.

Note that the mean first passage times shown in Figures 5 and 6 are in part subject to substantial noise due to insufficient statistical sampling: for example, clear deviations from a monotonously increasing function (expected for diffusive dynamics) are observed in the KCl-folding times shown in Figure 5a; this irregularity has its origin in an exceptionally long-lived (relative to the full trajectory duration) state of a specific peptide configuration in the KCl time series in Figure 1 within the time range 200 ns $\lesssim t \lesssim$ 400 ns. Briefly, this specific configuration is characterized by two helical turns and the Ace-cap being buried between the hydrophobic side chains of one Lys and one Ala group. This configuration (not involving bound ions) is found rather frequently in all trajectories but with typically much shorter life times.

Let us now turn to the interpretation of the mean folding times by the free energy $F(q)$ and diffusivity profiles $D(q)$. For

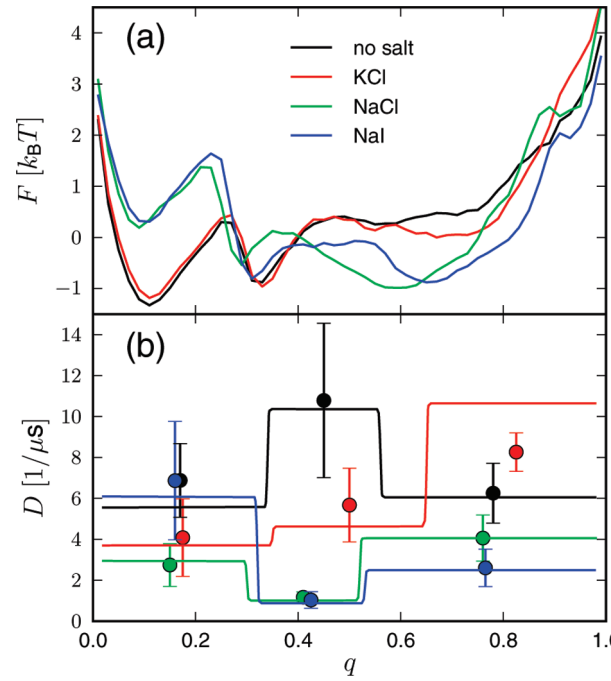


**Figure 7.** (a) Free energy landscapes (same as in Figure 2a). (b) Diffusivity profiles $D(q)$ for all investigated systems resolved by three regions $q < q_{2/3}$, $q_{2/3} \le q \le q_{1/3}$, and $q \ge {}_{1/3}$, which correspond to the fully helical, two-turn, and one-turn as well as unfolded states, respectively. Symbols including error bars result from fits to the ensemble of round-trip times $\tau_{RT}(q, q_t)$ for different targets $q_t$, while fitting results to the average round-trip time curve $\bar{\tau}_{RT}$ (eq 7) are displayed as solid lines.

statistical reasons leading to the above-mentioned anomalies, we have resolved the $D(q)$ profile only by three $q$ regions distinguishing between the three states: (1) mainly full-helix, (2) one- and two-turn states, and (3) mainly unfolded states. We assume that these states are separated by the $q$ values, where the average helicity is 2/3 and 1/3 in Figure 2 (the salt-specific values of $q_{2/3}$ and $q_{1/3}$ being summarized in Table 1). Although the resolution of $D(q)$ is small, we emphasize that it can almost quantitatively reproduce the folding and unfolding times plotted in Figures 5 and 6. Mean first passage times for folding and unfolding predicted by the FP equation involving salt-specific free energies and diffusivities are shown in the Supporting Information.

Figure 7 shows diffusivity profiles obtained by fitting to the average round-trip time defined in eq 7 (solid lines) and the $D(q)$ estimates resulting from fits to round-trip times of specific targets $q_t$ (symbols with error bars): first of all, we observe that they are not flat, a feature discussed previously for this peptide in the salt-free case.[8] The inhomogeneities reflect variations of the multidimensional configurational mobility of the peptide projected onto the one-dimensional RC $q$. Note also the fact that both analysis methods yield estimates, which coincide within error bars (the only exception being KCl for $q > q_{1/3}$), clearly validating our approach. After including the salt, a few significant changes to $D(q)$ are visible within the large error bars: first, in the solution with sodium salts there is a moderate decrease of the effective diffusivity by 30−60% in the large $q$ region, $q > q_{1/3}$, where the peptide is mostly unfolded. In contrast, with KCl the diffusivity seems to increase by 30−60% in the unfolded regions. Second, a drastic drop in diffusivity is observed for all salts in the central region $q_{2/3} < q < q_{1/3}$, where the peptide features one or two α-helical turns; the decrease is about *1 order of magnitude* for the sodium salts NaCl and NaI.

Finally, we find a smaller decrease of the diffusivity again in the completely folded states $q < q_{2/3}$, where the diffusion drops by about 30−60% for the KCl and NaCl salts.

Thus, while no clear-cut trends in the change of the diffusivity profile with salt can be recognized, clearly the diffusivity mainly decreases with salt, along with a significant drop in the partially folded states in the intermediate $q$ region. Importantly, the changes of $D(q)$ with salt are obviously not just a rescaling of $D(q)$ of the salt-free system as if the action would just stem from a nonspecific change due to a different bulk viscosity. In particular, the very few cases for which a viscosity argument applies could be for NaCl and KCl in the low $q$ region, $q < q_{2/3}$, or for NaCl and NaI in the high $q$ region, $q > q_{1/3}$: here the diffusivity is reduced by a factor of 2, roughly the same as for the viscosity increase (see Methods). Since there is no general trend, however, we must conclude that the change of the diffusivity profile originates from a combination of bulk viscosity effects *and* specific cosolute binding to the peptide. We believe that viscosity effects may be more important in the large $q$ region than in the low $q$ region: while large scale coil rearrangements in the solvent are frequent in the former, changes along the RC are mainly governed by internal mechanisms in the latter case; here only minor configurational rearrangements such as the expulsion of one water molecule or one ion, or the forming and breaking of internal hydrogen bonds, takes place. From this perspective it is interesting to see the diffusivity increase in the high $q$ region for KCl, while from viscosity arguments only it should decrease by a factor of 2.

However, given the diffusivity profiles in Figure 7, the large increase of folding times (Figures 5a and 6a) for the sodium salts must thus be attributed not only to the changes in the free energy landscape but, more dominantly, to the strongly reduced diffusivity in the intermediate $q$ region, $q_{2/3} \lesssim q \lesssim q_{1/3}$. The faster unfolding and the weaker dependence of unfolding vs folding times on salt type (cf. Figures 5b and 6b) seem to arise from a cancelation effect, where the small mobility in the intermediate $q$ regions is counterbalanced by the low unfolding barriers in $F(q)$ (a comparison of the FP description for average folding and unfolding times with the raw data shown in Figure 5 is given in the Supporting Information).

What are the molecular reasons for the major changes in the diffusivity profiles in the electrolytes solutions? On the basis of our structural and ion binding analysis in the previous section, it is now easy to argue that the huge drop in the effective diffusivity in the sodium salts is generated by the long-lived configurations similar to those shown in Figure 4. The long-lived character of these conformations is clearly observed in trajectory analysis and also manifested in the long binding times of cations on a nanosecond time scale as shown in Figure 3. While the form of the free energy landscape does not depend on the lifetime of these states (just what fraction of time they are sampled), the long life times are clearly reflected in parts of the diffusivity profiles. Due to the stronger binding of $Na^+$ vs $K^+$ to the peptide oxygen atoms, the effect is much smaller in the KCl solution than for the sodium salts.

## 4. Summary and Concluding Remarks

In summary, we have investigated the specific effects of salt at molar concentrations on the α-helical folding kinetics of a short, alanine-based and salt-bridge-forming peptide by means of molecular simulations and a diffusional analysis. Mean folding times have been found to considerably depend on salt type with folding times varying over 1 order of magnitude. The molecular basis for this is the previously observed stronger binding affinity of $Na^+$ vs $K^+$ ions to anionic peptide groups thereby transiently cross-linking multiple groups in the peptide. These binding processes increase the internal friction and induce a new, slow time scale. Within an analysis in terms of an effective diffusivity in a one-dimensional free energy landscape, these new time scales are expressed by a strong and salt-specific variation of the local diffusivity. A recent simulation study of a fully charged polyglutamic acid chain in salt solution showed that segmental relaxation kinetics were significantly slowed because of the same molecular mechanisms.[36]

Therefore, adsorption of ions not only alter the equilibrium but also kinetic properties of protein folding by direct binding mechanisms. Whether a general relation between preferential adsorption[52] and changes in kinetics can be drawn may be an interesting topic for further research. Given the current insights, it seems likely, however, that the change in kinetics not only depends on the amount of adsorbed ions but also on the nature of the individual ion−peptide interactions.

As we have demonstrated, molecular simulations can provide valuable information to understand the complex mechanisms in solvent−protein interactions and thereby protein stability and folding. The molecular mechanism found may be of general importance to understand cosolute effects on protein folding kinetics and shed more light onto experimentally observed cation-specific slowing of (bio)polyelectrolyte kinetics,[18,21] in particular, for halophilic proteins;[19,20] similar mechanisms may be at work in polymer melts.[53] More experimental studies are highly desirable; in particular, the novel long-lived loop-forming configurations in the denatured/unfolded states, in which sodium or similarly strong binders are bound and immobilized by the peptide backbone, may be experimentally accessible by nuclear magnetic relaxation dispersion methods (NMRD)[54] or time-resolved FRET measurement[12] probing salt-specific peptide relaxation and kinetics.

Furthermore, the action of complex denaturants such as guanidinium and urea deserve further attention, and systematic studies on specific salt effects should follow. The guanidinium cation, for instance, has been shown to decrease friction in neutral $(GlySer)_n$ peptides.[11,12] We expect also a strong influence of other specifically binding cations on anionic peptides, such as lithium, or polyvalent cations, such as $Mg^{2+}$ or $Ca^{2+}$. Large effects may also be anticipated by exchanging the anion; the latter has been found to considerably alter the unfolding kinetics of a halophilic protein.[19,20]

**Acknowledgment.** The authors are grateful to Michael Hinczewski and Roland R. Netz for useful discussions, the Deutsche Forschungsgemeinschaft (DFG) for support within the Emmy-Noether-Program (I.K. and J.D.) and the SFB 863 (Y.v.H. and J.D.), the CompInt graduate school for support within the Elitenetzwerk Bayern (Y.v.H.), and the Leibniz Rechenzentrum (LRZ) München for computing time on HLRB II.

**Supporting Information Available:** Details regarding the choice of a specific reference structure for the definition of the RC and concerning the fitting procedure to round-trip times employed to resolve diffusivity profiles. This material is available free of charge via the Internet at http://pubs.acs.org.

## References and Notes

(1) Bryngelson, J. D.; Wolynes, P. G. *J. Phys. Chem.* **1989**, *93*, 6902.

(2) Camacho, C. J.; Thirumalai, D. *Proc. Natl. Acad. Sci. U.S.A.* **1993**, *90*, 6369.

(3) Socci, N. D.; Onuchic, J. N.; Wolynes, P. G. *J. Chem. Phys.* **1996**, *104*, 5860.
(4) Dill, K. A.; Chan, H. S. *Nat. Struct. Biol.* **1997**, *4*, 10.
(5) Hummer, G.; Garcia, A. E.; Garde, S. *Phys. Rev. Lett.* **2000**, *85*, 2637.
(6) Best, R. B.; Hummer, G. *Phys. Rev. Lett.* **2006**, *96*, 228104.
(7) Best, R. B.; Hummer, G. *Proc. Natl. Acad. Sci. U.S.A.* **2010**, *107*, 1088.
(8) Hinczewski, M.; von Hansen, Y.; Dzubiella, J.; Netz, R. R. *J. Chem. Phys.* **2010**, *132*, 245103.
(9) Pabit, S. A.; Roder, H.; Hagen, S. J. *Biochemistry* **2004**, *43*, 12532.
(10) Cellmer, T.; Henry, E. R.; Hofrichter, J.; Eaton, W. A. *Proc. Natl. Acad. Sci. U.S.A.* **2008**, *105*, 18320.
(11) Buscaglia, M.; Lapidus, L. J.; Eaton, W. A.; Hofrichter, J. *Biophys. J.* **2006**, *91*, 276.
(12) Moglich, A.; Joder, K.; Kiefhaber, T. *Proc. Natl. Acad. Sci. U.S.A.* **2006**, *103*, 12394.
(13) Baldwin, R. L. *Biophys. J.* **1996**, *71*, 2056.
(14) Vrbka, L.; Vondrasek, J.; Jagoda-Cwiklik, B.; Vacha, R.; Jungwirth, P. *Proc. Natl. Acad. Sci. U.S.A.* **2006**, *103*, 15440.
(15) Uejio, J. S.; Schwartz, C. P.; Duffin, A. M.; Drisdell, W. S.; Cohen, R. C.; Saykally, R. J. *Proc. Natl. Acad. Sci. U.S.A.* **2008**, *105*, 6809.
(16) Aziz, E. F.; Ottosson, N.; Eisebitt, S.; Eberhardt, W.; Jagoda-Cwiklik, B.; Vacha, R.; Jungwirth, P.; Winter, B. *J. Phys. Chem. B* **2008**, *112*, 12567.
(17) Fedorov, M. V.; Goodman, J. M.; Schumm, S. *J. Am. Chem. Soc.* **2009**, *131*, 10854.
(18) Colaco, M.; Park, J.; Blanch, H. *Biophys. Chem.* **2008**, *136*, 74.
(19) Madern, D.; Ebel, C.; Zaccai, G. *Extremophiles* **2000**, *4*, 91.
(20) Bandyopadhyay, A. K.; Krishnamoorthy, G.; Padhy, L. C.; Sonawat, H. M. *Extremophiles* **2007**, *11*, 615.
(21) Gray, R. D.; Chaires, J. B. *Nucleic Acids Res.* **2008**, *36*, 4191.
(22) Dumetz, A. C.; Snellinger-O'Brien, A. M.; Kaler, E. W.; Lenhoff, A. M. *Protein Sci.* **2007**, *16*, 1867.
(23) Dyer, W. J. *Food Res.* **1951**, *16*, 522.
(24) Lanyi, J. K. *Bacteriol. Rev.* **1974**, *38*, 272.
(25) Karplus, M.; McCammon, J. A. *Nat. Struct. Biol.* **2002**, *9*, 646.
(26) Marqusee, S.; Baldwin, R. L. *Proc. Natl. Acad. Sci. U.S.A.* **1987**, *84*, 8898.
(27) Marqusee, S.; Robbins, V. H.; Baldwin, R. L. *Proc. Natl. Acad. Sci. U.S.A.* **1989**, *86*, 5286.
(28) Spek, E. J.; Olson, C. A.; Shi, Z. S.; Kallenbach, N. R. *J. Am. Chem. Soc.* **1999**, *121*, 5571.
(29) Chakrabartty, A.; Kortemme, T.; Baldwin, R. L. *Protein Sci.* **1994**, *3*, 843.
(30) Scholtz, J. M.; York, E. J.; Stewart, J. M.; Baldwin, R. L. *J. Am. Chem. Soc.* **1991**, *113*, 5102.
(31) Dzubiella, J. *J. Am. Chem. Soc.* **2008**, *130*, 14000.
(32) Case, D. A. AMBER9.0, University of California, San Francisco, 2006.
(33) Dang, L. X. *J. Am. Chem. Soc.* **1995**, *117*, 6954.
(34) Joung, I. S.; Cheatham, T. E. *J. Phys. Chem. B* **2008**, *112*, 9020.
(35) Kalcher, I.; Dzubiella, J. *J. Chem. Phys.* **2009**, *130*, 134507.
(36) Dzubiella, J. *J. Phys. Chem. B* **2010**, *114*, 7098.
(37) Kabsch, W.; Sander, C. *Biopolymers* **1983**, *22*, 2577.
(38) der Spoel, D. V.; Lindahl, E.; Hess, B.; Groenhof, G.; Mark, A. E.; Berendsen, H. J. C. *J. Comput. Chem.* **2005**, *26*, 1701.
(39) Lindahl, E.; Hess, B.; van der Spoel, D. *J. Mol. Model.* **2001**, *7*, 306.
(40) Hess, B. *J. Chem. Phys.* **2002**, *116*, 209.
(41) Zwanzig, R. *Annu. Rev. Phys. Chem.* **1965**, *16*, 67.
(42) Chen, T.; Smit, B.; Bell, A. T. *J. Chem. Phys.* **2009**, *131*, 246101.
(43) Gonzalez, M. A.; Abascal, J. L. F. *J. Chem. Phys.* **2010**, *132*, 096101.
(44) Robinson, R. A.; Stokes, R. H. *Electrolyte Solutions*, 2nd ed.; Dover Publications Inc.: Mineola, NY, 2002.
(45) Harris, K. R.; Woolf, L. A. *J. Chem. Eng. Data* **2004**, *49*, 1064.
(46) Hanggi, P.; Talkner, P.; Borkovec, M. *Rev. Modern Phys.* **1990**, *62*, 251.
(47) Metzler, R.; Klafter, J. *Chem. Phys. Lett.* **2000**, *321*, 238.
(48) Barrat, J.-L. Hansen, J.-P. *Basic Concepts for Simple and Complex Fluids*; University Press: Cambridge, 2003.
(49) Kou, S. C.; Xie, X. S. *Phys. Rev. Lett.* **2004**, *93*, 180603.
(50) Neusius, T.; Daidone, I.; Sokolov, I. M.; Smith, J. C. *Phys. Rev. Lett.* **2008**, *100*, 188103.
(51) Sangha, A. K.; Keyes, T. *J. Phys. Chem. B* **2009**, *113*, 15886.
(52) Parsegian, V. A.; Rand, R. P.; Rau, D. C. *Proc. Natl. Acad. Sci. U.S.A.* **2000**, *97*, 3987.
(53) Mos, B.; Verkerk, P.; Pouget, S.; van Zon, A.; Bel, G. J.; de Leeuw, S. W.; Eisenbach, C. D. *J. Chem. Phys.* **2000**, *113*, 4.
(54) Denisov, V. P.; Peters, J.; Horlein, H. D.; Halle, B. *Nat. Struct. Biol.* **1996**, *3*, 505.
(55) Humphrey, W.; Dalke, A.; Schulten, K. *J. Mol. Graphics* **1996**, *14*, 33.

JP107495F

# Supporting Information for "Ion-specificity in $\alpha$-helical folding kinetics"

Yann von Hansen, Immanuel Kalcher, and Joachim Dzubiella*
*Physics Department T37, Technical University Munich, 85748 Garching, Germany.*

Details on the sensitivity of the reaction coordinate to the reference structure and on the fitting procedure to round-trip times employed to resolve diffusivity profiles are provided in this supporting information.

## I. SENSITIVITY OF THE REACTION COORDINATE TO THE REFERENCE STRUCTURE

The specific choice of the microscopic reference structure used for the definition of the reaction coordinate (RC) $Q$ has only minor influence on the form of the resulting time series as is easily seen in Fig. S1, where the time series $q(t)$ is shown for three different structures for the salt-free case. Consequently, the resulting free energy landscapes obtained by Boltzmann-inversion of the time-averaged probability distribution (shown in Fig. S2) are only slightly perturbed when changing the reference state.

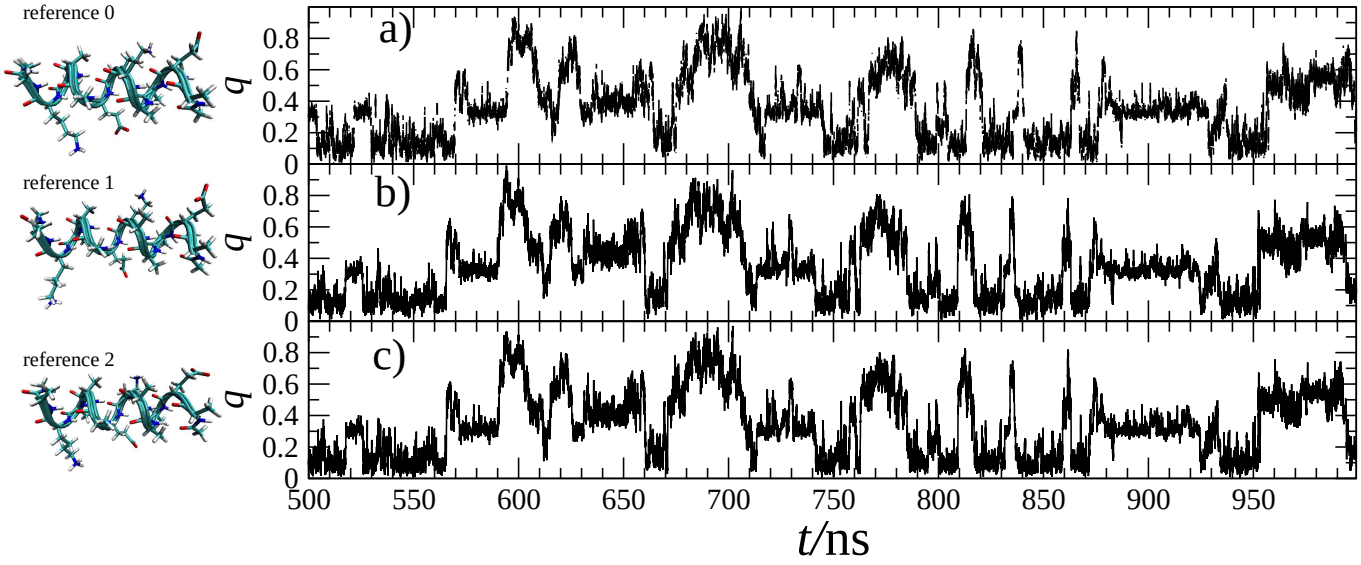


FIG. S1: Left: reference structures. Right: Time series of the RC $q(t)$ for several different choices of the reference structure. a) reference 0; b) reference 1; c) reference 2. The reference structures deviate from each other mainly in the arrangement of the E and K side chains. Reference structure 0 is the one used in the main body of work.

## II. ROUND-TRIP ANALYSIS

The round-trip function $\tau_{\mathrm{RT}}$ (Eq. (5) in the main text) is a function of $q$ involving four parameters: the target position $q_{\mathrm{t}}$, and the diffusivities $D^{\mathrm{f}}$, $D^{\mathrm{pf}}$, and $D^{\mathrm{uf}}$ in the folded region $q < q_{2/3}$, in the partially folded region $q_{2/3} \leq q < q_{1/3}$, and in the unfolded region $q \geq_{1/3}$, respectively, where the salt specific values of $q_{2/3}$ and $q_{1/3}$ are found in Tab. 1 in the main text.

Free energy landscapes for the systems with and without salt are shown in the panels (a) of Fig. S3; colored circles denote the positions of target points $q_{\mathrm{t}}$ considered in the round-trip time (RTT) analysis. RTTs extracted from the simulation trajectory $q(t)$ by combining mean first passage times according to Eq. (4) in the main text are shown as colored dots in the panels (b) of Fig. S3; the color-coding corresponds to the one of the target points in the panels (a).

*To whom correspondence should be addressed. E-mail: jdzubiel@ph.tum.de

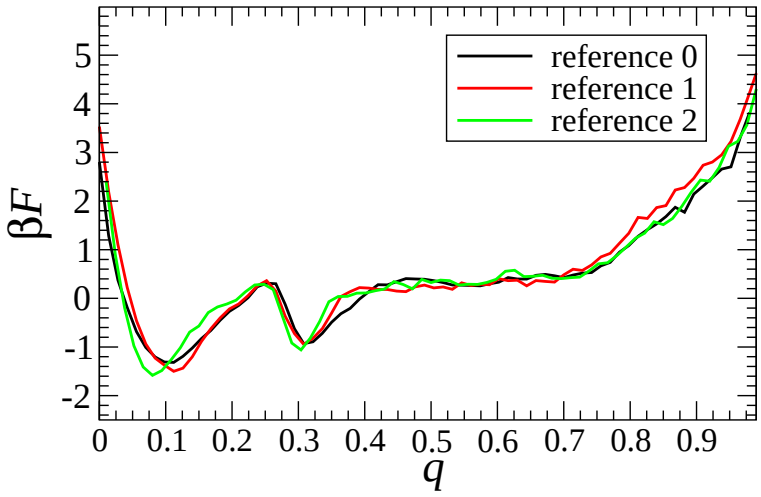


FIG. S2: Free energy landscapes resulting from the same choices of the reference structure as in Fig. S1.

The average round-trip curve is displayed as thicker red line. We now adjust the three diffusivity values $D^{\mathrm{f}}$, $D^{\mathrm{pf}}$, and $D^{\mathrm{uf}}$ in such a way to best reproduce the RTT data extracted from the simulation trajectory: best fits are shown as lines in the panels (b) of Fig. S3 (colored thin lines corresponding to fits to RTT data belonging to specific targets $q_{\mathrm{t}}$, and the thicker dashed black line showing the best fit to the average RTT defined in Eq. (7) in the main text). The diffusivity profiles belonging to these fits are shown in Fig. S3 (c) (again same color coding).

Note that insufficient statistical sampling and deviations from pure Markovian dynamics along $q$ lead to irregularities in the round-trip data of Fig. S3 (b): round-trip curves corresponding to distinct targets $q_{\mathrm{t}}$ are not just strictly shifted vertically w.r.t. each other (cf. Eq. (6) in the main text) and — in particular for KCl — non-monotonous behavior is observed for some of the targets (similarly to the artifacts seen in the average folding times in Fig. 5 in the main text). It is therefore not astonishing that the fit results yield diffusivities which vary considerably depending on the target position $q_{\mathrm{t}}$. The symbols with error bars in Fig. 7 (b) in the main text display means and standard deviations of the thin, colored diffusivity profiles in Fig S3 (c), while the solid lines display the fit results to the average RTT curve, which is less affected by statistical noise (thicker black lines in Fig S3 (c)).

Mean first passage times for folding and unfolding from the reduced Fokker-Planck (FP) approach using the free energy landscape and the diffusivity profiles obtained by fitting to $\bar{\tau}_{\mathrm{RT}}$ are compared in Fig. S4 to the raw simulation data (already shown in Fig. 5 of the main text). Note that the predictions of the reduced FP description are qualitatively in agreement with the simulation data (especially for longer times where non-Markovian effects become negligible), in contrast to what one would expect from a naive look at the different free energies. For comparison we show in Fig. S5 average folding and unfolding times resulting from a FP description involving a state-independent diffusivity, i.e. a diffusion *constant*.

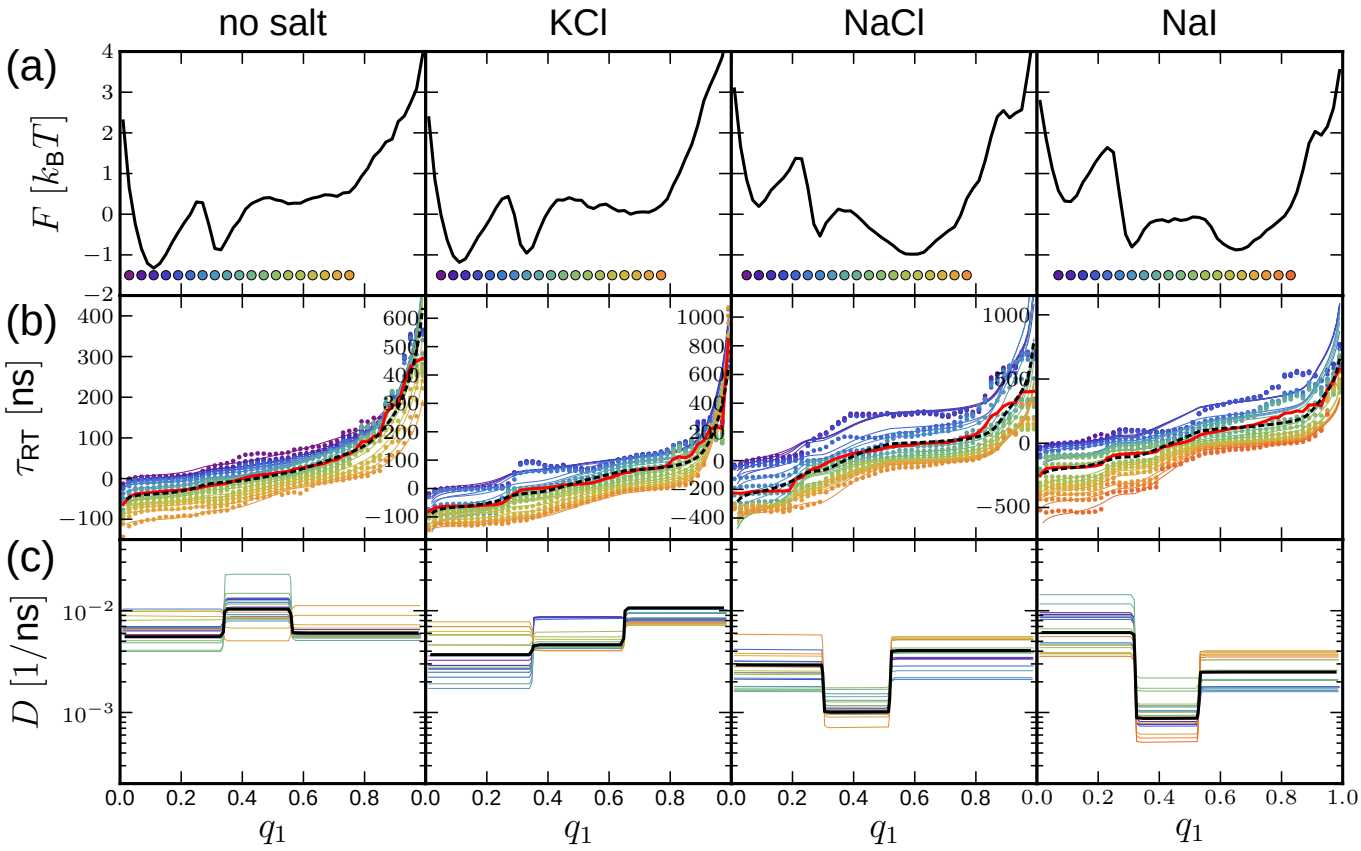


FIG. S3: (a) Free energy landscapes with and without salt; colored circles show the positions of the target points $q_\mathrm{t}$ considered in the round-trip time analysis. (b) Round-trip times from the $q(t)$ trajectory (colored dots, same color coding as in (a)); colored lines show best fits of the round-trip time functions to the simulation data. Averaged round-trip data (Eq. (5) in the main text) is shown as thick red line, the best fit is displayed as broken black line. (c) Diffusivity profiles resulting from best fits to the data shown in panel (b).

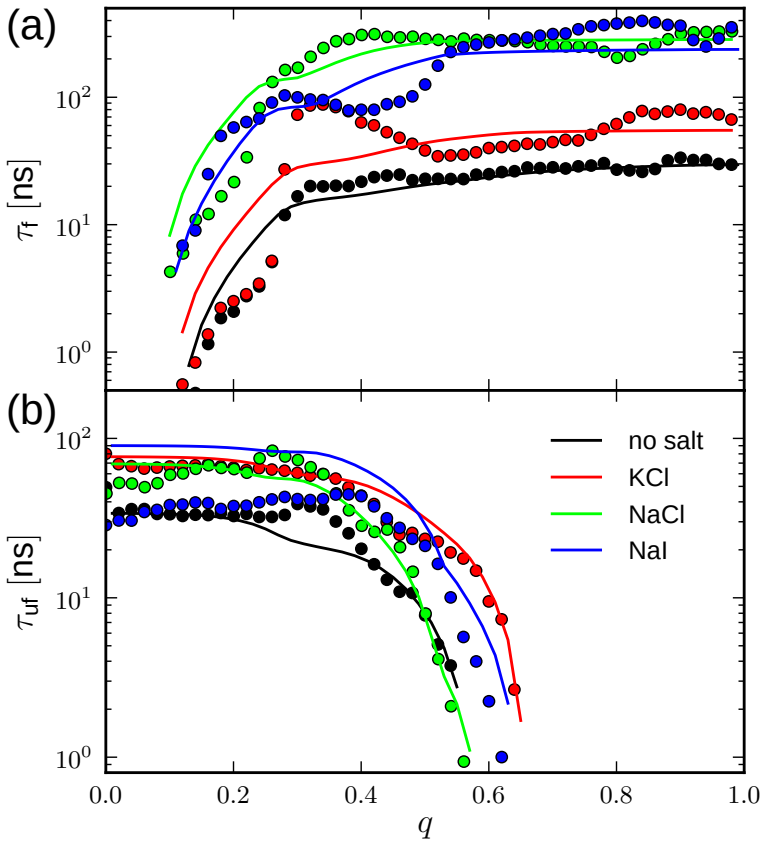


FIG. S4: (a) Average folding times from the reduced FP description using the diffusion profiles denoted by solid lines in Fig. 7 of the main text (*lines*) and from the original time series (*circles*, data already shown in Fig. 5 (a) of the main text). (b) Average unfolding times (cf. Fig. 5 (b) in the main text).

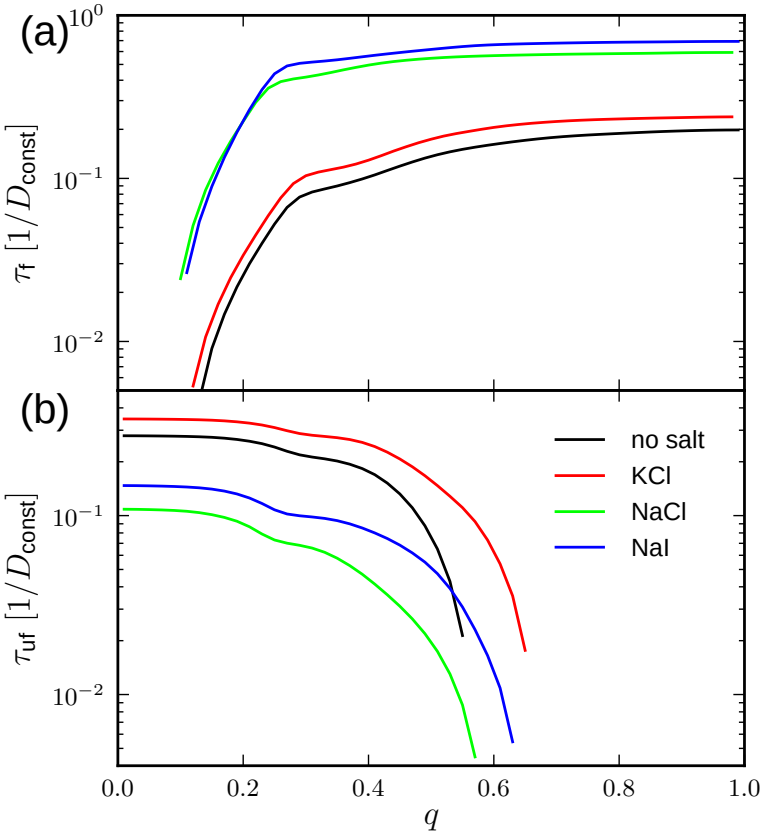


FIG. S5: (a) Average folding and (b) average unfolding times from the reduced FP description assuming a flat diffusivity profile; times are shown in units of the inverse diffusion constant $D_{\mathrm{const}}$.